Journal of Materials Chemistry B

ROYAL SOCIETY OF CHEMISTRY

PAPER

View Article Online
View Journal | View Issue

Cite this: J. Mater. Chem. B, 2026, 14, 4037

Drop-on-demand antimicrobial printed coatings loaded with a dehydroabietic acid derivative to prevent orthopedic implant infections

David Martínez-Pérez,†[a] Inés Reigada,†[b] Jayendra Z. Patel,[c] Jari Yli-Kauhaluoma,[c] Leena Hanski,[b] Michał Srebrzynski,[de] Maciej Spychalski,[a] Emilia Choińska,[a] Adyary Fallarero[b] and Wojciech Święszkowski*[a]

Received 25th September 2025,
Accepted 5th March 2026

DOI: 10.1039/d5tb02177d

rsc.li/materials-b

Microvalve-based drop-on-demand (DOD) printing technology was applied to create antimicrobial coatings for orthopedic implants. Leveraging the high-precision deposition capabilities of DOD, coatings loaded with a novel biofilm inhibitor, *N*-(abiet-8,11,13-trien-18-oyl) cyclohexyl-L-alanine (DHA1), were fabricated on titanium coupons. The PLGA-PEG-DHA1 coatings exhibited significant efficacy in preventing *Staphylococcus aureus* adhesion in mono- and co-cultures with HL-60 cells. Furthermore, the PLGA-PEG-DHA1 coatings showed a sustained protective effect of the 30% DHA1-loaded coating over 24 hours. The PLGA-PEG-DHA1 coatings ensured safety with no cytotoxic effect observed on SaOS-2 mammalian cells, fostering tissue integration post-implantation. This study highlights the potential for the future production of multi-component DOD coatings combining various ink compositions, including different polymers, antimicrobial agents, or growth factors.

1 Introduction

The number of orthopedic surgeries has exponentially increased in recent years due to an aging population, increased prevalence of musculoskeletal disorders, and advancements in surgical techniques.[1] As the number of implantations continues to increase, there is a simultaneous rise in the incidence of implant failures, leading to patient distress and imposing a substantial economic burden.[2,3] Aseptic loosening and biomaterial-associated infection (BAI) stand out as the primary culprits behind implant failure,[2,4] 80% of the latter being caused by bacterial biofilms.[5,6] Implantable devices provide an optimal surface for bacteria to attach to and form a biofilm. This phenotypical switch aids pathogenic bacterial evasion of the immune defenses of the host and resistance to antibiotic treatment.

The implanted devices represent an ideal surface for bacteria to adhere to and form biofilms. A biofilm can protect bacteria from being recognized and phagocytosed by the host's immune cells and withstand antibiotic chemotherapy.[7] The primary microorganisms responsible for orthopedic infections are Gram-positive cocci, particularly those belonging to the *Staphylococcus* genus, with *Staphylococcus aureus* being the most prevalent.[8]

Prophylactic systemic antibiotics may be administered before device implantation to prevent peri-operative infection. Nevertheless, this method might pose challenges due to adverse effects in different bodily regions[9] and limited blood supply to the tissue where the implant is located. Systemic administration leads to a limited antibiotic concentration in the desired area. An approach to address this issue involves the creation of implants that release antimicrobials, enabling localized administration of these agents at the implantation site. In recent years, some commercial implant-related solutions were developed by focusing on the local delivery of antimicrobial compounds, such as sponges of collagen (Collatamp, EUSA Pharma), calcium sulfate beads (Stimulan, Biocomposites), bone cement (Palacos, Heraeus Medical),[10] and coated intramedullary nails (PROtect, DePuySynthes).[11] Antimicrobial agents can be incorporated onto the implants by using different coating techniques, such as impregnation, entrapment, dip coating, spraying, or painting.[12] However, these techniques have some limitations, such as low accuracy, low thickness control, use of high amounts of antimicrobial agents, or difficulties in combining two or more antimicrobial compounds. Current coating methods lack precision, limit the combination of multiple agents, and often require

[a] Faculty of Materials Science and Engineering, Warsaw University of Technology, Poland. E-mail: wojciech.swieszkowski@pw.edu.pl
[b] Drug Research Program, Division of Pharmaceutical Biosciences, Faculty of Pharmacy, University of Helsinki, Finland
[c] Drug Research Program, Division of Pharmaceutical Chemistry and Technology, Faculty of Pharmacy, University of Helsinki, Finland
[d] Department of Transplantology and Central Tissue Bank, Medical University of Warsaw, Poland
[e] National Centre for Tissue and Cell Banking, Warsaw, Poland
† David Martínez-Pérez and Inés Reigada contributed equally to this work.

high drug loadings. Thus, a precise, low-waste, and customizable method is urgently needed to create more effective antimicrobial implant coatings. Drop-on-demand (DOD) printing technology solves most of these limitations.

DOD is an excellent technology for high-accuracy deposition and patterning of materials. The actuator in the DOD system generates pulses that trigger the ejection of a specific volume of material from the reservoir. There are three methods of generating the pulses: (1) inkjet thermal-based, where a heater heats and evaporates a small amount of ink for a very short period, in the range of several microseconds, creating a bubble that drives the ejection of the material; (2) inkjet piezoelectric-based, where a voltage-applied on a piezoelectric actuator generates a mechanical deformation that triggers the ejection of the material;[13] (3) microvalve-based, where the system pressurizes the ink in the reservoir and applies an electric pulse to a valve coil. This electric pulse generates a magnetic field that pulls a plunger upwards, moving the nozzle and ejecting a droplet.[14] The capacity to deposit small fluid volumes while maintaining complete digital control and exact deposition at fast speeds makes DOD printing technology more precise than other coating techniques. The droplet deposition process may be designed such that subsequent solvent evaporation leads to the creation of a thin polymeric coating layer. In recent years, DOD printing has broadened its applications beyond traditional ink-on-paper printing into medical fields such as pharmaceuticals[15] (high-throughput drug screening for toxicology studies,[16,17] drug formulation[18] and oral dose development[19,20]), biomaterials,[21] and medical devices.[22]

One of the challenges met while preventing BAIs is that the narrow range of compounds can effectively target biofilms at adequately low concentrations,[23] given that when bacteria switch into the biofilm state, they can be up to a factor of 1000 more resistant to antibiotic therapy.[24] Our laboratory has embraced the search for new biofilm inhibitors *via* chemical screening, which has led to identification of dehydroabietic acid (DHA). This abietane-type diterpenoid effectively prevents the biofilm formation of staphylococcal biofilms at low concentrations. Moreover, only 2- to 4-fold higher concentrations of it are needed to reduce a pre-established biofilm.[25] The further optimization of this molecule led to the synthesis of *N*-(abiet-8,11,13-trien-18-oyl)cyclohexyl-L-alanine (DHA1), which managed the same anti-biofilm activity of DHA at significantly lower concentration.[26]

In the present work, poly(D,L-lactide-*co*-glycolide) (PLGA) was selected as the main structural matrix of the coating due to its established use in implantable drug delivery systems, providing mechanical integrity, adhesion to titanium substrates, and controlled degradation. Poly(ethylene glycol) (PEG) was incorporated in a minor fraction to modulate surface hydrophilicity, enhance cytocompatibility, and facilitate the release of the bioactive compound. This combination enables the development of stable, biocompatible coatings with tunable release properties while maintaining printability.

To our knowledge, this is the first study to apply microvalve-based DOD printing for depositing DHA1, a novel biofilm inhibitor, onto titanium surfaces, yielding precise, patterned, and tunable antimicrobial coatings. The objective of this study was to develop and optimize DOD-printed PLGA-PEG coatings incorporating DHA1, and to evaluate their antimicrobial efficacy, release behavior, and cytocompatibility as a proof-of-concept for preventing orthopedic implant infections.

In this work, DOD printing coatings loaded with DHA1 (0%, 10%, 20%, and 30%) were produced. The antimicrobial performance of the created coatings was evaluated by examining their capability to hinder *S. aureus* adhesion when tested in both monoculture and co-culture with HL-60 cells. To determine the antimicrobial potential of the eluates over time and their compatibility with relevant mammalian cell lines, a release assay was conducted.

2 Materials and methods

2.1. Materials

Poly(D,L-lactide-*co*-glycolide) (PLGA) Purasorb PDLG 5004A, PDLG 5010, and PDLG 7507 were purchased from Corbion (Amsterdam, the Netherlands). PLGA 5–10 kDa (AP081) and 10–15 kDa (AP041) were acquired from PolySciTech, Akina Inc. (West Lafayette, IN, United States). Chloroform was acquired from Stanlab (Lublin, Poland). Anisole and poly(ethylene glycol) (PEG, 35 kDa) were acquired from Sigma-Aldrich (St Louis, MO, the United States). Titanium coupons (diameter 12.7 mm, thickness 3.8 mm) were acquired from Biosurface Technologies Corporation (Bozeman, MT, United States).

2.2. GPC analysis

Molecular masses of polymers were measured using gel permeation chromatography. The modular system Agilent 1200 series HPLC equipped with two PLgel 5 μm MIXED-C columns (300 mm, 7.5 mm) in series and a refractive index detector (RID) was used. Calibration was carried out using 12 narrow-distributed polystyrene (PS) standards, which had molecular weights (M_p) ranging from 474 to 1 800 000 Da. Analysis was conducted at a temperature of 35 °C, using HPLC-grade chloroform as the solvent with a flow rate of 0.7 mL min^{-1}. Prior to the analysis, all the samples, approximately 2.5 mg mL^{-1}, were passed through a 0.2 μm PTFE syringe filter.

2.3. Rheological and printability screening

The rheological properties of different polymer formulations were studied by dissolving the polymers in anisole at different concentrations and analyzed with a viscometer (DV-III Ultra, Brookfield), using a cone disc CPA-40Z at 100 and 250 rpm at 22 °C. The printability was analyzed using a DOD printer (3D Discovery, regenHU) and a jetting printing head (∅ = 150 μm), evaluating the correct formation and deposition of the droplets and avoiding the formation of satellites or clogging of the nozzle. Samples were evaluated using a digital microscope (Keyence, VHX-7000).

2.4. DOD ink preparation and plasma surface activation

PLGA (PDLG 5004A) (9%) and PEG (1%) were mixed into a solution of chloroform and anisole (3 : 1). DHA1 was added to

the solutions at different concentrations (0, 10, 20, or 30% w/w). The inks were transferred into a 3 mL syringe and loaded into the printer.

To increase the wettability, the surface of titanium coupons was treated by low-pressure plasma (Zepto, Diener, Ebhausen, Germany). The parameters were optimized through time, power (60–120 W), and gases used (Ar, O_2). The water contact angle and surface energy of the titanium coupons were measured with a goniometer (OCA20, Dataphysics, Germany) using water and diiodomethane as probe liquids, and the surface energy was calculated according to the Owens–Wendt method.

2.5. DOD printed coatings and characterization

Titanium coupons were surface activated by oxygen plasma at 120 W for 1 min. PLGA-PEG-DHA1 coatings were produced using a microvalve-based DOD printer (3D Discovery, regenHU). The optimized printing parameters were 200 μs VOT (valve opening time), 125 ms VCT (valve closing time), 0.1 MPa reservoir pressure, and 3 mm distance nozzle-sample. Samples were left at room temperature and pressure overnight for solvent evaporation and then transferred into a low-pressure chamber for five days for complete evaporation of organic residues. Samples were placed in multiwell plates and irradiated using gamma radiation with doses of 25 kGy according to ISO 11137-2. Gamma sterilization was performed using a Co-60 gamma irradiator (ISOGAMMA-LLCo, Hungary). The irradiation of the samples was carried out in a cylindrical, stainless steel sample holder with thermal isolation, and the empty space was filled up with ground dry ice. The printability and roughness were evaluated using a digital microscope (Keyence, VHX-7000). A magnification of 500× and L-filter of 2.5 mm were used to measure the linear (R_a) and area roughness (S_a). The composition of the coatings was studied using Fourier-transform infrared (FTIR) spectroscopy in the ATR mode using a Nicolet 8700 (Thermo Fisher Scientific). Spectra were collected in the range of 500 to 4000 cm^{-1}, data spacing 0.482 cm^{-1} and number of scans 32. The reduced Young's modulus of PLGA-PEG and PLGA-PEG-DHA1 coatings was analyzed using a Hysitron system equipped with a Berkovitz nanoindenter. The parameters used were a maximum load of 150 μN, a loading rate of 15 μN s^{-1}, and 2 s of loading.

2.6. Bacterial strains

Gram-positive bacteria *Staphylococcus aureus* ATCC 25923 were used for the antimicrobial assessment of the developed coatings. They were stored at −80 °C in tryptic soy broth (TSB) containing 20% glycerol, and prior to experimentation were grown on tryptone soy agar plates (TSA, Neogen®, Lansing, MI, USA), overnight (37 °C, aerobic conditions).

2.7. Mammalian cell maintenance

HL-60 cells (ATCC CCL-240) were cultivated at a concentration ranging from 1×10^5 to 1×10^6 cells per mL. They were cultured in Roswell Park Memorial Institute (RPMI) 1640 Medium (R8758), supplemented with 10% (v/v) heat-inactivated fetal bovine serum (FBS) and 1% (v/v) penicillin/streptomycin (all of which were purchased from Sigma-Aldrich, St Louis, MO, USA). To differentiate them into polymorphonuclear-like cells, they were cultured for six days in the described RPMI media supplemented with 100 mM *N*,*N*-dimethylformamide (DMF; Sigma Aldrich, St Louis, MO, USA).[27]

The SaOS-2 cells (89050205, European Collection of Authenticated Cell cultures, ECACC), which are a human osteosarcoma cell line, were maintained in minimum essential medium (MEM; Sigma-Aldrich, St Louis, Missouri, USA). The culture medium was supplemented with 500 IU per mL penicillin, and 0.1 mg mL^{-1} streptomycin (both antibiotics were purchased from Sigma-Aldrich, St Louis, Missouri, USA) and 10% (v/v) FBS.

Both cell lines were maintained at 37 °C in 5% CO_2 in a humidified incubator in 72 cm^2 culture flasks (VWR, Radnor, PA, USA).

2.8. Impact of the coatings on bacterial adhesion

Titanium coupons coated with PLGA-PEG-DHA1 (Control, 10%, 20%, and 30%) were introduced in 24 well plates (Nunclon surface, Nunc, Roskilde, Denmark). A mid-exponential culture of *S. aureus* in tryptic soy broth (TSB, Neogen®, Lansing, Michigan, USA) was diluted to approximately 1×10^6 CFU mL^{-1} in TSB and added to each well. Following a 24-hour incubation period (220 rpm, 37 °C), each coupon was immersed in TSB to eliminate planktonic bacteria and then transferred into 1 mL of sterile TBS with 0.5% Tween20®. To dislodge the bacteria, a cycle of 20 s vortexing was applied to each tube, after which it was sonicated at 35 kHz (20 °C) for 5 min using an Ultrasonic Cleaner 3800 water sonicator (Branson Ultrasonics, Danbury, CT, USA), and then vortexed for an additional 20 s.

Dilutions 1 : 10 to 1 : 10^8 were then made from each resulting bacterial suspension in TSB and 10 μL of each dilution was plated onto tryptic soy agar (TSA, Neogen®, Lansing, MI, USA). The plates were dried and incubated for less than 24 hours, after which the viable colonies were quantified.

2.9. Impact of the coatings on bacterial adhesion in a co-culture including *S. aureus* ATCC 25923 and neutrophil-like HL-60

Following the protocol of ref. 28 1 mL of a 1 : 1 mixture of a mid-exponential suspension of *S. aureus* ATCC 25923 (2×10^7 CFU mL^{-1}) and a suspension of differentiated HL-60 cells (2×10^5 cells per mL) were added onto titanium coupons with different coatings were placed in the wells of a 24-well plate. Both suspensions were in RPMI. To prepare the bacterial suspension, *S. aureus* was grown in TSB and washed twice with sterile phosphate-buffered saline (PBS). The bacterial concentration was adjusted to 2×10^8 CFU mL^{-1} in RPMI *via* absorbance measurement at 595 nm and further diluted to 2×10^7 CFU mL^{-1}. In the case of the HL-60 cells, 24 h prior to the experiment, the media were refreshed with RPMI without antibiotics. For the experiment, cell concentration was adjusted to 2×10^5 cells per mL in RPMI.

The coupons were incubated in this mix of bacterial and cell suspension for 24 h at 37 °C, 5% CO_2 in an incubator with humidity control, after which the viable attached bacteria were quantified as described in Section 2.10.

2.10. Release assay

Titanium coupons with the different coatings were placed on a 24-well plate and 1 mL of non-supplemented MEM was added to each coupon. At the specific timepoints, the complete volume was removed and stored (at −20 °C) for further testing. The collected volume was replaced with fresh media at each timepoint. The release was performed in a humidified incubator (37 °C, 5% CO_2).

2.10.1. Antimicrobial and anti-biofilm effects of the released eluates. The antimicrobial and antibiofilm activity of the eluates was assessed by combining 20 μL of a *S. aureus* suspension in TSB with (1×10^7 CFU mL^{-1} of a mid-exponential culture) 180 μL of each eluate, the final bacterial concentration being 1×10^6 CFU mL^{-1} per well in a 96 well plates (Nunclon surface, Nunc, Roskilde, Denmark). After incubation (18 h, 37 °C, 220 rpm), the metabolic activity of both planktonic bacteria and biofilms was measured following a protocol from a previous work.[29] The bacterial suspension was transferred to a new 96-well plate and the turbidity was measured at 595 nm using a microplate spectrophotometer (Multiskan Sky, Thermo Scientific, Waltham, MA, USA). The biofilms formed on the plate were washed twice with 200 μL of PBS per well, after which a 20 μM resazurin solution in PBS was added (200 μL per well) and incubated for 20 min (RT, 220 rpm). After incubation, the fluorescence was measured at $\lambda_{excitation}$ = 560 nm and $\lambda_{emission}$ = 590 nm using a microplate reader (Varioskan LUX Multimode, Thermo Scientific, Waltham, MA, USA).

2.10.2. Cytotoxicity of the released eluates. A day prior to the experiment, SaOS-2 cells were seeded in 96-well plates at a density of 6×10^3 cells per well, corresponding to approximately 1.9×10^4 cells per cm^2. After incubation, 180 μL of each eluate and 10 μL of FBS were added per well. After the addition of the eluate (two technical replicates each) the cells were incubated for 24 h. Later, two washing cycles with PBS (200 μL per well) were performed, and 200 μL of a 20 μM resazurin solution were added per well. The plate was incubated for 2 h and measured the fluorescence as was described in the previous Section 2.10.1. All the incubation steps were done at 37 °C, 5% CO_2 in an incubator with humidity control.

3 Results and discussion

3.1. Surface plasma activation

The development of polymeric coatings on orthopedic implants has revolutionized the field of medical implants, enhancing their biocompatibility and antimicrobial functionality. Increasing the surface energy enhances the wettability of the implant before applying the polymeric coating. This strategy is commonly used for better adhesion, more uniform, and more durable coatings. Enhancing the wettability of the titanium surface facilitates a more even spread of the coating material. Different techniques can be used to enhance the surface energy on titanium, such as plasma activation, abrasion, laser, primers, or others. In this work, a low-pressure plasma was used to activate the surface of titanium coupons. The effect on the surface energy using oxygen and argon gas at 60 W and 120 W was studied. When the titanium was activated using oxygen plasma, the surface energy increased from 52 mN m^{-1} up to 69 and 71 mN m^{-1} at 60 W and 120 W, respectively. Utilizing argon plasma resulted in an increase of the surface energy, achieving 61 and 70 mN m^{-1} at 60 W and 120 W, respectively (Fig. 2). Oxygen gas and a power of 120 W were used for the activation of titanium coupons in further experiments.

3.2. Rheological analysis and DOD printability

We performed a study on the rheological properties and the printability of different inks based on PLGA (different molecular weights and lactic : glycolic ratio) and PLA at different concentrations (Table S1). The apparent viscosity was evaluated using a digital viscometer dissolving the polymers in anisole (Fig. 3b). The obtained experimental data fit an exponential growth equation, which is common in semi-dilute and concentrated polymeric solutions (Fig. S7).[30] A variety of formulations, using different polymers and solvents, were utilized to evaluate the printability of the microvalve-based DOD printer. The

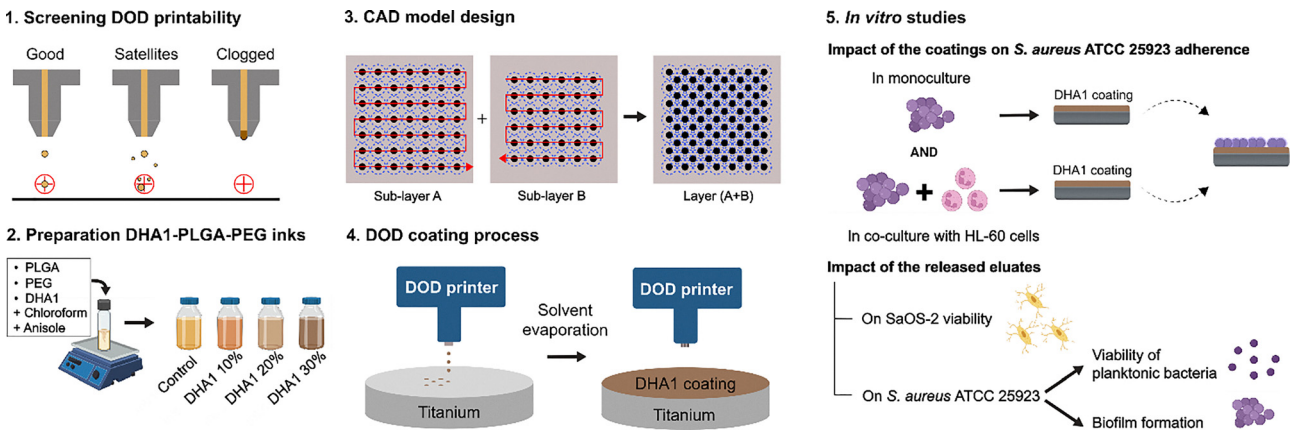

Fig. 1 DOD-DHA1 coating process. (1) Screening of different polymeric formulations with good printability and selection. (2) Development of a set of four inks: Control, DHA1 10%, DHA1 20%, and DHA1 30%. (3) Design of CAD model for deposition of droplets in two overlapped sub-layers. (4) DOD coating process on titanium coupons of DHA1 formulations. (5) *In vitro* studies of mono- and co-cultures of *S. aureus* ATCC25923 and HL-60 cells.

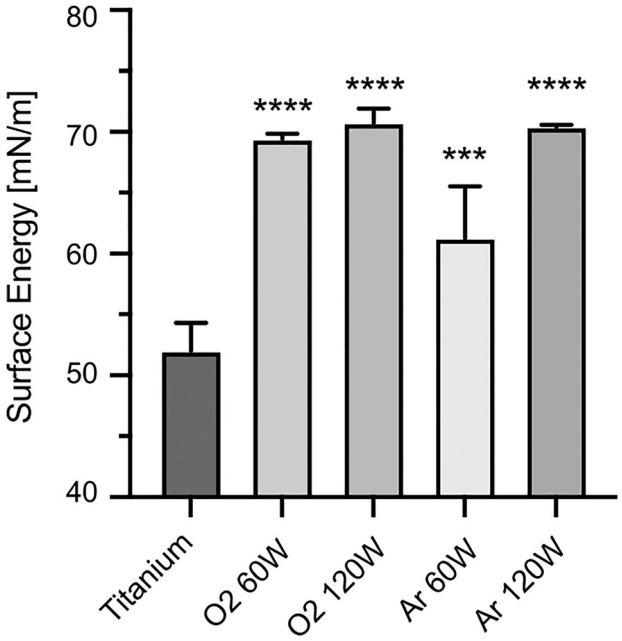

Fig. 2 Surface energy of titanium coupons activated by oxygen or argon plasma. Values are mean and SD (*$p < 0.05$;** $p < 0.01$; ***$p < 0.001$).

printability experiments were performed by dissolving PLGA and PLA in pure anisole. We observed a small printability window in the range between 7 and 24 mPa s of apparent viscosity, where the droplet formation and deposition were correct and reproducible. Below 7 mPa s, the formation of satellites and splashes was eventually observed. Above 24 mPa s, the nozzle usually got clogged, and no droplet formation was observed. This narrow viscosity range corresponds to a limited range of polymer concentrations suitable for optimal printing using microvalve-based DOD printing. A printability map (Fig. 3a) was obtained experimentally evaluating the correct droplet formation using macroscopic evaluation and a digital optical microscope. We observed that the mean concentration of the printability window decreases as the molecular weight of the polymers increases. In general, we observed a restricted range of viscosities to obtain an optimal printability using microvalve-based DOD technology. This finding underscores the necessity to maintain the proper balance within these parameters to ensure successful printing results. These results may be helpful in the future development of new inks using different polymers or blends.

Due to its extensive use in drug delivery applications and GMP production, PLGA (PDLG 5004A) was selected for further experiments. Furthermore, it is crucial to note that the incorporation of compounds, such as antibiotics, nanoparticles, growth factors, or any other substances, may have an impact on the viscosity of the solution, and hence, this consideration is vital to ensure optimal printability.

Due to the low volatility of anisole, an alternative solvent was required to develop the final formulation. Chloroform was explored as a potential alternative, as it is volatile, and PLGA and DHA1 are soluble in it. We observed that when using chloroform, the deposited droplets showed the typical "coffee ring" effect (Fig. S2a). This effect is produced during the drying process of the droplet due to a flow (Marangoni flow) from the center to the edge of the droplet. As the liquid evaporates, the polymer is deposited at the edges of the droplet, forming a ring-like pattern. The coffee ring effect can present some drawbacks that can affect the quality and functionality of the printed coatings. As most of the polymer is deposited at the borders, it creates a non-uniform distribution of the polymer on the substrate, leading to irregular and non-uniform coatings. To mitigate the coffee ring effect, different strategies can be employed, such as combining solvents with different volatilities,[31] loading nanoparticles or nanoflakes,[32,33] controlling the substrate properties,[34] and environmental/drying control. In this work, to solve the coffee ring effect, a mixture of chloroform and anisole was combined, in a ratio of 3 : 1. This mixture of solvents with different volatilities was found to be very effective in eliminating the coffee ring effect on the deposited droplets (Fig. S2b) and was used in further experiments.

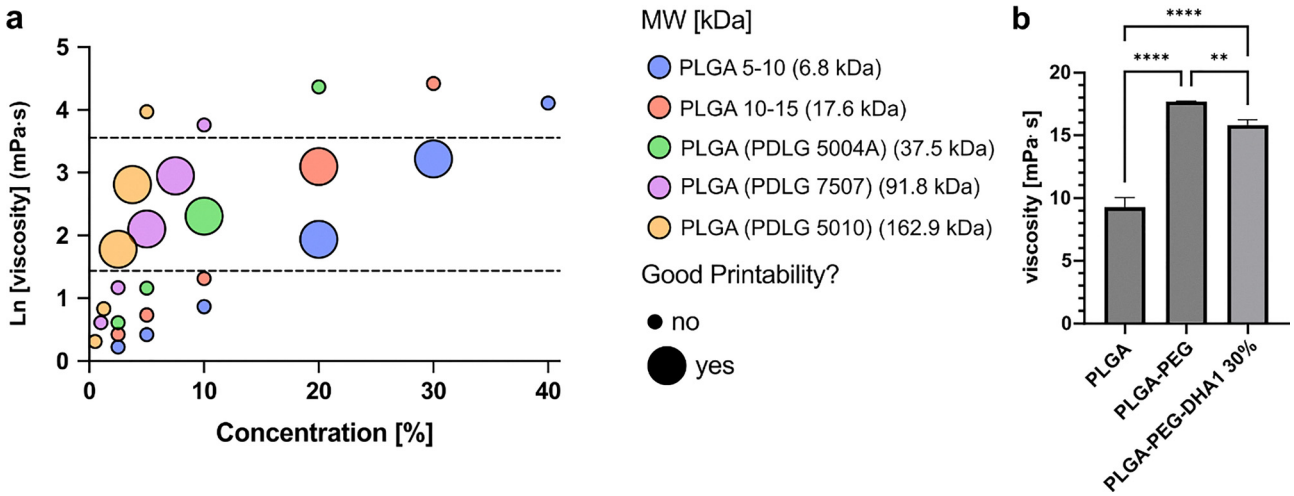

Fig. 3 (a) Screening printability map of inks of PLGA 5-10a (6.8 kDa), PLGA10-15a (17.6 kDa), PLGA (PDLG 5004A (37.5 kDa)), PLGA (PDLG 7507 (91.8 kDa)), or PLGA (PDLG 5010 (162.9 kDa)) for microvalve DOD printing technology. (b) Viscosity in anisole of PLGA 5004A 10% (w/v), PLGA 5004A (9% w/v) + PEG (1% w/v), and PLGA 5004A (9% w/v) + PEG (1% w/v) + DHA1 (30% w/w) ($n = 3$).

3.3. Optimization, development of DOD printed coatings and characterization

A final formulation of PLGA (PDLG 5004A) 9% (w/v) and PEG 1% (w/v) was developed. In this formulation, PLGA acts as the main coating matrix, while PEG is included as a secondary component to improve biocompatibility and modulate the release behavior of DHA1 without compromising coating stability or printability.[35] Rheological analysis of PLGA-PEG and PLGA-PEG-DHA1, 30% in pure anisole, was performed, confirming the viscosity of both inks within the printability range. The incorporation of PEG increased the viscosity of the ink from 9.27 ± 0.76 for PLGA 10% (w/v) to 17.67 ± 0.05 mPa s for PLGA 9% and PEG 1% (w/v) (Fig. S2). Ink formulations loaded with DHA1 (0%, 10%, 20%, and 30%) were prepared in a mixture of chloroform and anisole (Table 1). The excellent printability of the final formulation was confirmed by depositing a 5-layer matrix droplet (Fig. S2c), and the droplet profile confirmed a good droplet deposition and solvent evaporation with no coffee ring effect (Fig. S2d).

The valve opening time (VOT) of the nozzle was optimized. VOTs below 150 μs led to non-droplet formation (100 μs) or low precision of droplet deposition (125 μs). We observed that the volume of the deposited droplet increased while increasing the VOT (Fig. S2i). The CAD model was designed with a distance of 800 μm between droplets. The diameter of the deposited droplet increased (Fig. S3a) proportional to VOT, leading to an increased overlapping of droplets at higher VOTs. A VOT of 150 μs produced a patterned and uniform coating (Fig. S2e), while higher VOTs of 175, 200, and 225 μs produced non-uniform coatings due to excessive droplet overlapping (Fig. S2f, g and h).

A CAD model was designed to deposit droplets in a patterned matrix with a very slight overlapping between droplets, defined as a sub-layer A (see Fig. 1. CAD model design, and Fig. 4a). Then, a second pattern, defined as sub-layer B, was designed to fill the gaps in sub-layer A. Furthermore, at the time of printing sub-layer B, the droplets from the previous sub-layer A were mostly evaporated, avoiding the fusion of the droplets between sub-layers. This approach allowed us to create highly patterned coatings, confirmed *via* the optical microscope profile (Fig. 4b, c and f). The development of highly patterned coatings unlocks novel approaches to producing multi-component DOD coatings combining different printing heads and ink compositions, including different polymers, antimicrobial agents, or growth factors.

We demonstrated that the thickness of the coatings can be tuned with high precision, by controlling the number of printed layers in the CAD model. The thickness of a single layer was 1.46 ± 0.15 μm (mean ± SD) (Fig. 4d). The nanoindentation reduced Young's modulus values for Ti-PLGA-PEG, Ti-PLGA-PEG-DHA1 10%, Ti-PLGA-PEG-DHA1 20%, and Ti-PLGA-PEG-DHA1 30%, which are presented in Fig. 4f. The Ti-PLGA-PEG-DHA1 30% coating displays a consistently higher modulus compared to other coatings, suggesting a potential concentration-dependent effect of DHA1 on the mechanical properties. This finding aligns with previous studies on the impact of solute concentration on material stiffness, emphasizing the role of molecular interactions in governing mechanical behavior.[36] The reduced Young's modulus observed for the PLGA-PEG-DHA1 coatings compared to bare titanium is not expected to adversely affect the mechanical performance of the implant under physiological loading conditions. Given the micrometric thickness of the coating, the load-bearing behavior remains dominated by the titanium substrate, whose elastic modulus is several orders of magnitude higher. Instead, the lower modulus of the polymeric coating may be beneficial at the interface by reducing stiffness mismatch and promoting mechanical compatibility with surrounding tissues, without compromising the structural integrity of the implant.

The chemical analysis of the coatings was performed by FTIR in ATR mode. The spectra of pure PLGA (PDLG 5004A), PEG, DHA1, and printed coatings (control, 10%, 20%, and 30%) are shown in Fig. S1. Pure PLGA showed the characteristic peaks at 1745 and 1084 cm^{-1}, belonging to C═O stretching of the carbonyl group and C–O stretching, respectively.[37] When pure PEG was analyzed, it showed characteristic peaks at 2878, 1093, and 840 cm^{-1}, belonging to C–H stretching, O–H and C–O–H stretching, and CH_2 rocking, respectively.[38,39] The spectrum of pure DHA1 showed a peak at 3328 cm^{-1} belonging to the stretching of –OH hydroxyl groups and the stretching of –NH– secondary amines. The peaks at 2920 and 1731 cm^{-1} belong to the stretching of –C– carbons and the stretching of C═O of the carbonyl groups, respectively. The spectra of PLGA-PEG-DHA1 coatings showed similar characteristic peaks to PLGA. The characteristic peaks of PEG were not observed, as the most intense peaks overlapped with PLGA characteristic peaks. Furthermore, the incorporation of DHA1 was confirmed by the presence of the characteristic peaks of DHA1 (3328, 2920, 1624, and 1522 cm^{-1}) in the coatings of DHA1 10%, 20%, and 30%.

In future research studies, utilizing highly patterned DOD printed coatings may be an approach to produce multi-component coatings without resulting in unwanted mixing of the inks. Even though the application of combined inks in antimicrobial DOD printing for orthopedic implants has not been explored yet, our past research study has illustrated the benefits of employing a dual antibiotic delivery system in 3D-printed extruded hydrogels to combat antibiotic-resistant bacteria.[40]

Table 1 Microvalve-based formulation of DOD inks of PLGA-PEG (PDLG 5004A) loaded with 0% (control), 10%, 20%, or 30% DHA1

Ink	PLGA (PDLG5004) [%] (w/v)	PEG [%] (w/v)	DHA1 [%] (w/w)
Control	9	1	0
DHA1 10%	9	1	10
DHA1 20%	9	1	20
DHA1 30%	9	1	30

3.4. PLGA-PEG-DHA1 coatings prevent bacterial adhesion on titanium and do not impair the protective activity of HL-60 cells on bacterial adhesion

The minimum inhibitory concentration (MIC) of the DHA1 against *S. aureus* ATCC 25923 was assessed before and after sterilization by gamma radiation. As shown in Table S2, the

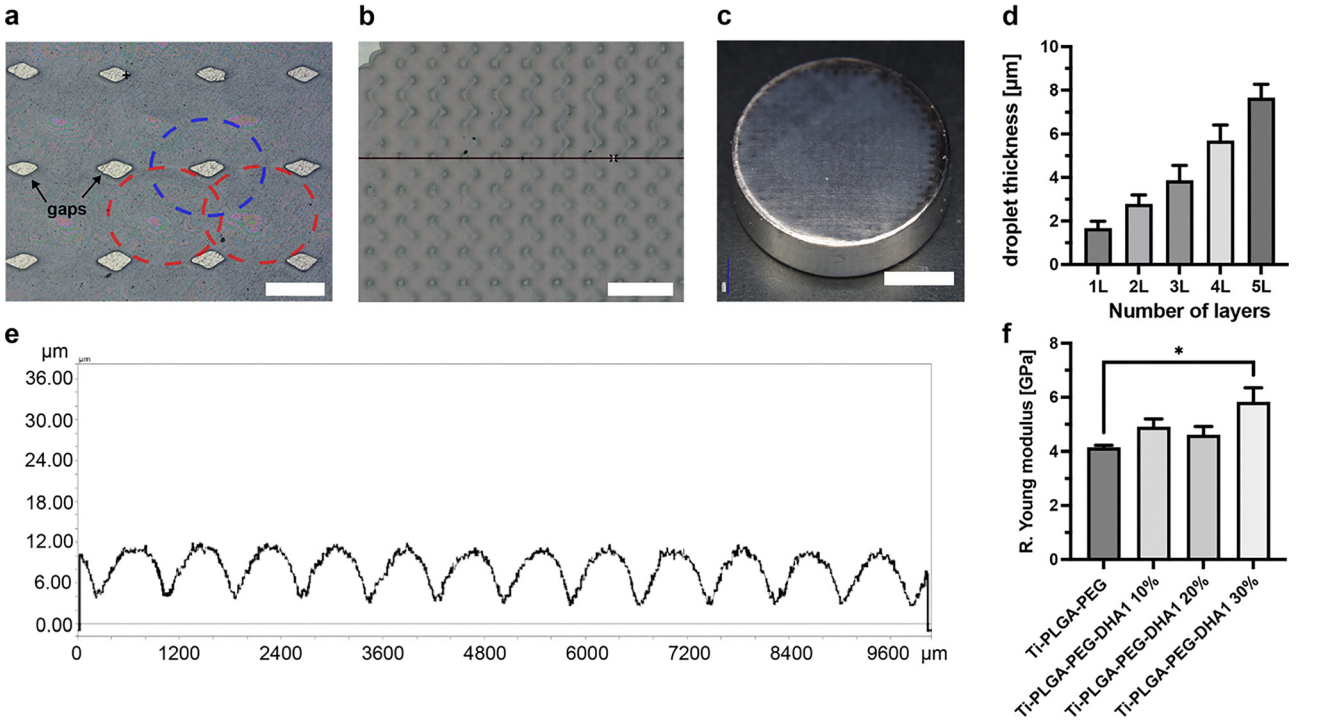

Fig. 4 (a) 1 sub-layer A DOD printed using PLGA-PEG-DHA1 ink. The red circles point to the areas of deposited droplets in sub-layer A, while the blue circle points to the areas where droplets are deposited in sub-layer B covering the gaps. (b) Optical 3D reconstruction and (e) 5-layer (A + B) PLGA-PEG-DHA1 coating profile. (c) Titanium coupon DOD coated by PLGA-PEG-DHA1. (d) Droplet thickness at different numbers of printed layers. (e) Profile of a DOD-printed PLGA-PEG-DHA1 coating on titanium. (f) Reduced Young modulus analyzed by Nano-indenter. Values are expressed as means and SD of five replicates. The scale bars are (a) 500 µm, (b) 2 mm, (c) 4 mm.

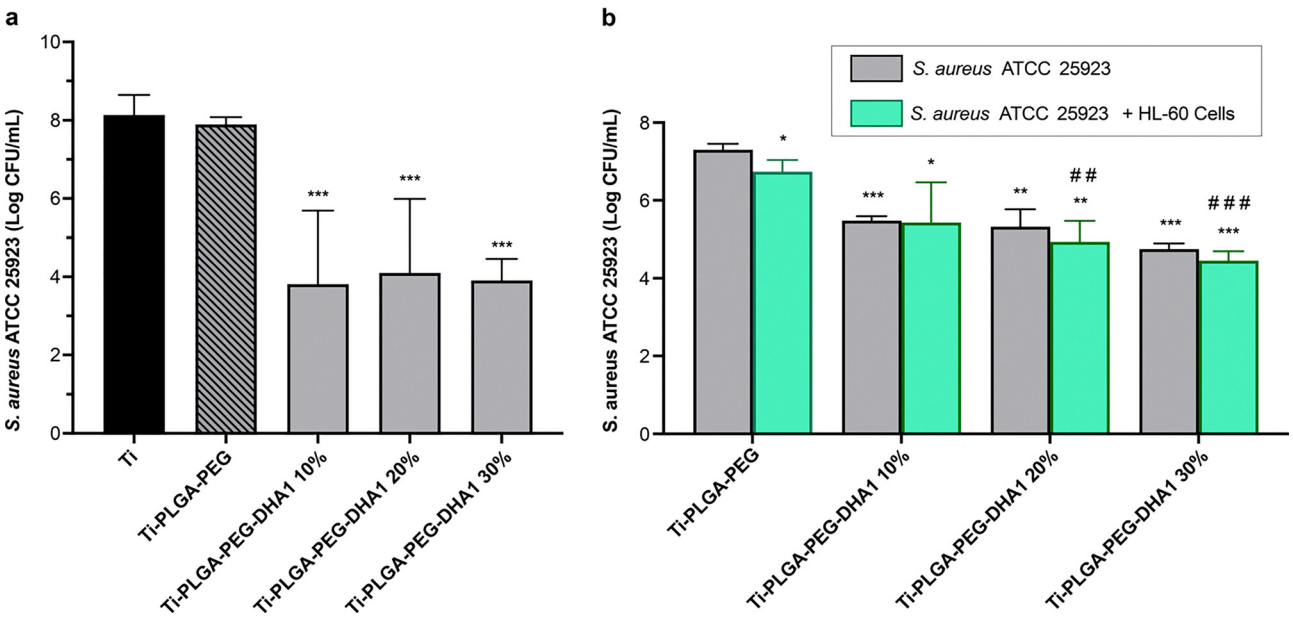

Fig. 5 *S. aureus* ATCC 25923 viable counts adhered to Ti, Ti-PLGA-PEG, Ti-PLGA-PEG-DHA1 10%, Ti-PLGA-PEG-DHA1 20%, and Ti-PLGA-PEG-DHA1 30% in mono-(a) and in HL-60 cells co-culture (b). The symbol "*" stands for differences between group and control in monoculture, and "#"for differences between group and control in co-culture. Student's *t*-test (*$p < 0.05$; **$p < 0.01$; ***$p < 0.001$)/($^{\#\#}p < 0.01$; $^{\#\#\#}p < 0.001$). Values are expressed as mean of the log CFU mL^{-1} and SD of three biological repetitions. The control group (Ti) corresponds to uncoated titanium samples.

sterilization did not affect the MIC of the DHA1. Fig. 5a shows the effects of the coatings incorporating different concentrations of DHA1 on the adherence *of S. aureus* ATCC 25923 to titanium surfaces. The Ti-PLGA-PEG did not show any difference from the uncoated titanium, so it was concluded that the PLGA-PEG coatings do not affect bacterial attachment.

Conversely, all of the Ti-PLGA-PEG-DHA1 coatings (10%, 20%, and 30%) managed an almost 4-log reduction on the *S. aureus* attachment ($p < 0.0001$).

It must be pointed out that the bacterial concentration used here was considerably high (1×10^6 CFU mL^{-1}), given that in clinical settings, a bacterial concentration of 1×10^4 CFU mL^{-1} is sufficient to generate infection during surgery, and only 10^2 CFU mL^{-1} are needed when a medical device is present.[41] This points towards a potential success in a clinical scenario, as the bacterial reduction achieved in these settings is very significant, even at high bacterial concentrations.

One reason for the lower bacterial concentration required to initiate an infection when a medical device is present is the impaired function of granulocytes due to the presence of a foreign material. This impairment occurs because the surgery damages the surrounding tissue, leading to the release of damage-associated molecular patterns (DAMPs), which are molecules that signal danger and activate the immune system of the host.[42] After the detection of DAMPs, neutrophils and macrophages travel to the damaged tissue where they try to clear out the foreign material.[43] When these defense mechanisms fail to break down the material, it results in cell exhaustion and death, eventually creating an immune-suppressed environment around the implant. This immune suppression makes the material more susceptible to microbial colonization and biofilm-mediated infections.[44] For these reasons, to guarantee the efficacy of the antimicrobial coating in the clinic, it is essential to predict the effects of the coatings on the bacteria clearance capacity of innate immune cells.

Fig. 5b shows the effects of the different coatings on bacterial adhesion when tested in a co-culture system of bacterial and innate immune cells. In accordance with previous findings, the presence of HL-60 cells reduced the bacterial adherence ($p = 0.043$, when comparing the mono- and co-culture controls, grey and green columns, respectively). All the coatings significantly prevented bacterial adherence in monocultures, and the coatings at 20% and 30% seemed to further reduce bacterial attachment when they were combined with HL-60 cells.

These results demonstrate that none of the different coatings impaired the antimicrobial capacity of neutrophils. While no statistically significant enhancement relative to monoculture conditions was observed, the DHA1-loaded coatings maintained their antibacterial efficacy in the presence of HL-60 cells, indicating that the coatings are compatible with innate immune cell function. This is of great importance, as it has been previously observed that coatings displaying promising antimicrobial capacity *in vitro* may fail to protect against infection *in vivo* due to toxic effects on innate immune cells.[45]

3.5. Cytotoxicity study of released eluates on mammalian cells

Unspecific cytotoxicity is a concern that is common to all antimicrobials, but it becomes even more relevant in the case of implanted devices. In combination with infection, aseptic loosening is a leading cause of implant failure.[46] For this reason, it is essential to ensure that the incorporated antimicrobial would not hamper the tissue integration. Furthermore, the swift establishment of host cells within the implant not only promotes tissue integration but also serves as a defense against infection.[47] This underscores the importance of minimizing any toxic effects on the tissue cells.

In Fig. 6 the impact of the released eluates on SaOS-2 cell viability can be seen. It is observed that none of the different coatings at any time point produced any toxic effect on this cell line, with the percentage of viability consistently above 90%, which may indicate that the developed coatings would not hamper tissue integration.

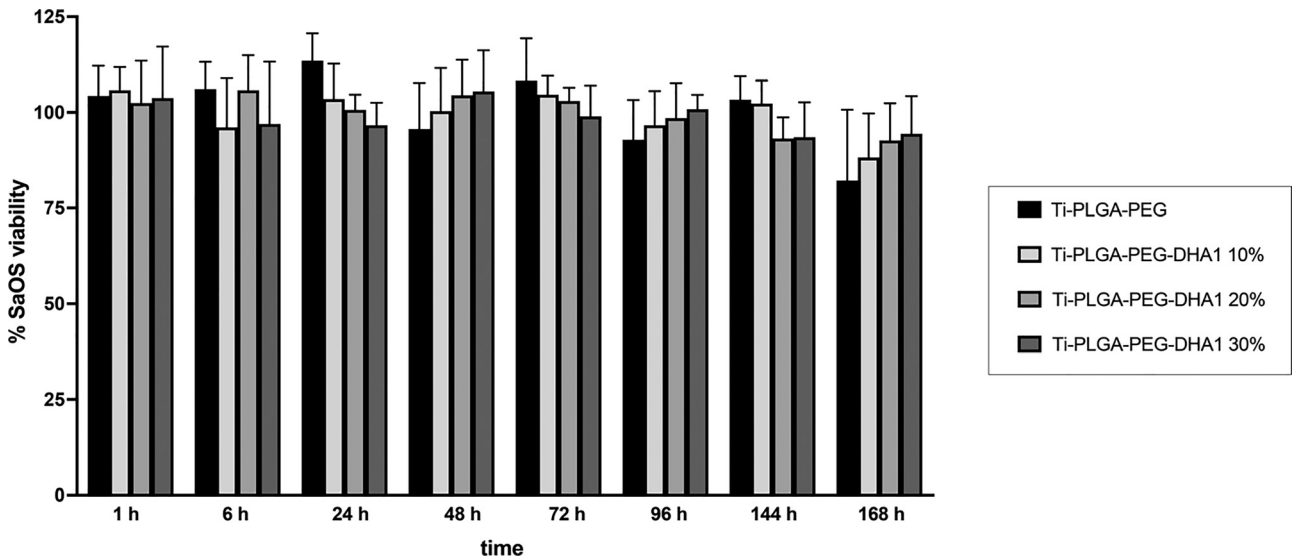

Fig. 6 Effects of the eluates of Ti-PLGA-PEG, Ti-PLGA-PEG-DHA1 10%, Ti-PLGA-PEG-DHA1 20%, and Ti-PLGA-PEG-DHA1 30% on the SaOS-2 cell viability. The viability was obtained using Ti untreated coupons as control after 24 h incubation on. Values are means and SD of two biological repetitions.

3.6. Antimicrobial and antibiofilm impact of the released eluates

The analysis of drug release rate is essential in the development of a drug delivery coating. Quantitative determination of DHA1 release was attempted using UV-Vis spectroscopy as well as amine-reactive assays, including fluorescence-based methods. However, reliable quantification could not be achieved. As a result, release behavior was evaluated using a functional approach based on the antimicrobial and antibiofilm activity of the collected eluates over time. While this method does not provide absolute release quantities, it allows assessment of the biological relevance and duration of antimicrobial activity associated with DHA1 release from the coatings.

The antimicrobial activity of the released eluates was evaluated at different time points up to 72 hours. As described in the Materials and methods section, the whole volume of media was taken and refilled with the same volume per time-point. This experiment evaluates not only the protection of the material against infection but also of the surrounding tissue.[48] During the first 6 hours, all the eluates managed to significantly inhibit the planktonic bacterial growth (Fig. 7a) ($p = 0.014$; $p = 0.001$ and $p = 0.013$, comparing 10, 20, and 30% with the bacterial control) and the biofilm formation (Fig. 7b) ($p < 0.001$, in all cases). However, it is only the eluate corresponding to the coating with 30% DHA1, the one guaranteeing protection for up to 24 hours, as it manages around 50% inhibition of the planktonic bacteria growth ($p < 0.001$, Fig. 7a) and above a 50% inhibition of the biofilm formation ($p < 0.001$, Fig. 7b). The DHA1 loading of 30% was selected as the highest concentration evaluated, as it provided the strongest antibacterial performance while maintaining stable ink formulation and reliable printability using the microvalve-based DOD system. Higher DHA1 loadings were not pursued due to limitations related to ink viscosity and droplet formation, which are critical parameters for reproducible DOD printing. Importantly, the 30% DHA1 formulation has already achieved a substantial reduction in bacterial adhesion and sustained antimicrobial activity, making further increases in DHA1 content unnecessary for the objectives of this study. These results demonstrate that DHA1 30% coatings can effectively prevent biofilm formation and planktonic bacteria growth for up to 24 hours after implantation.

4 Conclusions

In this work, a novel formulation of PLGA-PEG-DHA1 was demonstrated for use in additive manufacturing of antimicrobial orthopedic implants. DOD printing was applied to produce patterned antimicrobial coatings with high-precision geometries and thickness control. PLGA-PEG-DHA1 coatings were shown to be very effective in preventing biofilm formation in monoculture and co-culture with HL-60 cells. The drug release assay demonstrated an effective prevention of biofilm formation and inhibition of planktonic bacteria for the first 24 hours after implantation. This work also shows the way to develop new ink formulations using different polymers, opening the possibility of developing more complex ink formulations, *e.g.*, a combination of antimicrobial compounds, ions, growth factors, *etc.* Applying two or more printing heads and combining different ink formulations may be the future research direction to develop highly controlled drug delivery

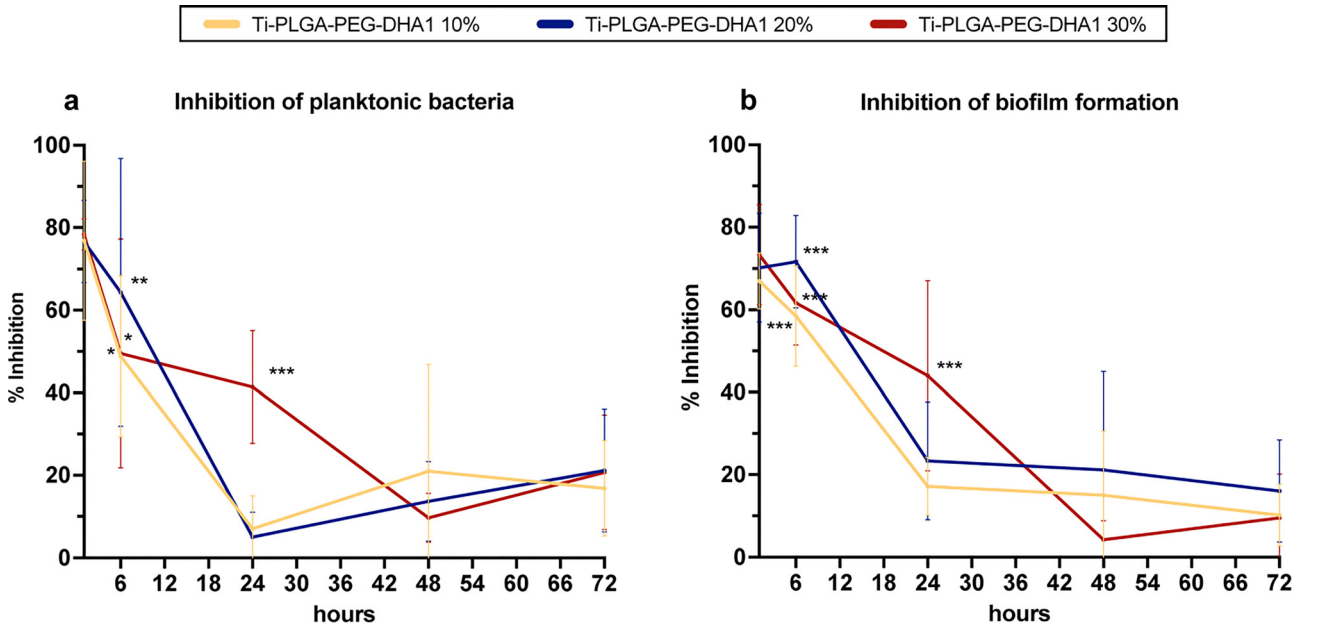

Fig. 7 Percentage of inhibition of planktonic bacteria (a) and formation of biofilm (b) at various time points, 100% as untreated control (*$p < 0.05$; ** $p < 0.01$; ***$p < 0.001$). Data are presented as mean ± standard deviation from two independent biological replicates, each measured in triplicate (three technical replicates per biological replicate).

systems, potentially revolutionizing therapeutic applications in orthopedic implants.

Conflicts of interest

The authors have no known competing financial or personal interests that could influence the work reported in this paper.

Data availability

The data supporting the findings of this study are available from the corresponding author upon reasonable request.

The supplementary information includes additional tables and figures supporting this study, including rheological and printability data, FTIR spectra, surface characterization, MIC values, and supplementary experimental results. See DOI: https://doi.org/10.1039/d5tb02177d.

Acknowledgements

This research was funded by the EU Framework Program for Research and Innovation H2020 – MSCA Training Networks, Print-Aid project and grant number 722467, the National Centre for Research and Development, MATURO 3D project and grant number TECHMATSTRATEG2/407770/2/NCBR/2020, and the Academy of Finland (grant numbers 333291 to L. H. and 322724 to J. Z. P.).

References

1 S. Veerachamy, T. Yarlagadda, G. Manivasagam and P. K. Yarlagadda, Bacterial adherence and biofilm formation on medical implants: a review, *Proc. Inst. Mech. Eng., Part H*, 2014, **228**(10), 1083–1099, DOI: 10.1177/0954411914556137.
2 S. M. Kurtz, E. Lau, H. Watson, J. K. Schmier and J. Parvizi, Economic burden of periprosthetic joint infection in the United States, *J. Arthroplasty*, 2012, **27**(8 suppl), 61–5.e1, DOI: 10.1016/j.arth.2012.02.022.
3 M. G. Kaufman, J. D. Meaike and S. A. Izaddoost, Orthopedic Prosthetic Infections: Diagnosis and Orthopedic Salvage, *Semin. Plast. Surg.*, 2016, **30**(2), 66–72, DOI: 10.1055/s-0036-1580730.
4 C. R. Arciola, D. Campoccia and L. Montanaro, Implant infections: adhesion, biofilm formation and immune evasion, *Nat. Rev. Microbiol.*, 2018, **16**(7), 397–409, DOI: 10.1038/s41579-018-0019-y.
5 S. L. Percival, L. Suleman, C. Vuotto and G. Donelli, Healthcare-associated infections, medical devices and biofilms: risk, tolerance and control, *J. Med. Microbiol.*, 2015, **64**(Pt 4), 323–334, DOI: 10.1099/jmm.0.000032.
6 H. A. Khan, F. K. Baig and R. Mehboob, Nosocomial infections: Epidemiology, prevention, control and surveillance, *Asian Pac. J. Trop. Biomed.*, 2017, **7**(5), 478–482, DOI: 10.1016/j.apjtb.2017.01.019.
7 J. W. Costerton, P. S. Stewart and E. P. Greenberg, Bacterial biofilms: A common cause of persistent infections, *Science*, 1999, **284**(5418), 1318–1322, DOI: 10.1126/science.284.5418.1318.
8 C. R. Arciola, D. Campoccia, G. D. Ehrlich and L. Montanaro, Biofilm-based implant infections in orthopaedics, *Adv. Exp. Med. Biol.*, 2015, **830**, 29–46, DOI: 10.1007/978-3-319-11038-7_2.
9 F. Jahanmard, *et al.*, Bactericidal coating to prevent early and delayed implant-related infections, *J. Controlled Release*, 2020, **326**, 38–52, DOI: 10.1016/j.jconrel.2020.06.014.
10 N. Kavanagh, *et al.*, Staphylococcal Osteomyelitis: Disease Progression, Treatment Challenges, and Future Directions, *Clin. Microbiol. Rev.*, 2018, **31**(2), e00084-17, DOI: 10.1128/CMR.00084-17.
11 T. Fuchs, R. Stange, G. Schmidmaier and M. J. Raschke, The use of gentamicin-coated nails in the tibia: preliminary results of a prospective study, *Arch. Orthop. Trauma. Surg.*, 2011, **131**(10), 1419–1425, DOI: 10.1007/s00402-011-1321-6.
12 in *Antimicrobial Coatings and Modifications on Medical Devices*, ed. Z. Zhang and V. E. Wagner, Springer International Publishing, Cham, 2017, DOI: 10.1007/978-3-319-57494-3.
13 T. Jungst, W. Smolan, K. Schacht, T. Scheibel and J. Groll, Strategies and Molecular Design Criteria for 3D Printable Hydrogels, *Chem. Rev.*, 2016, **116**(3), 1496–1539, DOI: 10.1021/acs.chemrev.5b00303.
14 H. Gudapati, M. Dey and I. Ozbolat, A comprehensive review on droplet-based bioprinting: Past, present and future, *Biomaterials*, 2016, **102**, 20–42, DOI: 10.1016/j.biomaterials.2016.06.012.
15 S. E. Evans, T. Harrington, M. C. Rodriguez Rivero, E. Rognin, T. Tuladhar and R. Daly, 2D and 3D inkjet printing of biopharmaceuticals – A review of trends and future perspectives in research and manufacturing, *Int. J. Pharm.*, 2021, **599**, 120443, DOI: 10.1016/j.ijpharm.2021.120443.
16 M. Choi, J. Hwang, J. Choi and J. Hong, Multicomponent High-throughput Drug Screening via Inkjet Printing to Verify the Effect of Immunosuppressive Drugs on Immune T Lymphocytes, *Sci. Rep.*, 2017, **7**(1), 6318, DOI: 10.1038/s41598-017-06690-2.
17 I. D. Styliari, *et al.*, High-Throughput Miniaturized Screening of Nanoparticle Formation via Inkjet Printing, *Macromol. Mater. Eng.*, 2018, **303**(8), 1800146, DOI: 10.1002/mame.201800146.
18 N. Scoutaris, M. R. Alexander, P. R. Gellert and C. J. Roberts, Inkjet printing as a novel medicine formulation technique, *J. Controlled Release*, 2011, **156**(2), 179–185, DOI: 10.1016/j.jconrel.2011.07.033.
19 C. W. Rowe, W. E. Katstra, R. D. Palazzolo, B. Giritlioglu, P. Teung and M. J. Cima, Multimechanism oral dosage forms fabricated by three dimensional printingE, *J. Controlled Release*, 2000, 7.
20 W. E. Katstra, R. D. Palazzolo, C. W. Rowe, B. Giritlioglu, P. Teung and M. J. Cima, Oral dosage forms fabricated by Three Dimensional PrintingE, *J. Controlled Release*, 2000, 9.
21 K. Tappa and U. Jammalamadaka, Novel Biomaterials Used in Medical 3D Printing Techniques, *J. Funct. Biomater.*, 2018, **9**(1), 17, DOI: 10.3390/jfb9010017.

22 Y. He, *et al.*, A Reactive Prodrug Ink Formulation Strategy for Inkjet 3D Printing of Controlled Release Dosage Forms and Implants, *Adv. Ther.*, 2020, **3**(6), 1900187, DOI: 10.1002/adtp.201900187.
23 M. Jaskiewicz, A. Janczura, J. Nowicka and W. Kamysz, Methods Used for the Eradication of Staphylococcal Biofilms, *Antibiotics*, 2019, **8**(4), 174, DOI: 10.3390/antibiotics8040174.
24 G. Gebreyohannes, A. Nyerere, C. Bii and D. B. Sbhatu, Challenges of intervention, treatment, and antibiotic resistance of biofilm-forming microorganisms, *Heliyon*, 2019, **5**(8), e02192, DOI: 10.1016/j.heliyon.2019.e02192.
25 A. Fallarero, *et al.*, (+)-Dehydroabietic acid, an abietane-type diterpene, inhibits Staphylococcus aureus biofilms in vitro, *Int. J. Mol. Sci.*, 2013, **14**(6), 12054–12072, DOI: 10.3390/ijms140612054.
26 S. Manner, *et al.*, New derivatives of dehydroabietic acid target planktonic and biofilm bacteria in Staphylococcus aureus and effectively disrupt bacterial membrane integrity, *Eur. J. Med. Chem.*, 2015, **102**, 68–79, DOI: 10.1016/j.ejmech.2015.07.038.
27 S. J. Collins, F. W. Ruscetti, R. E. Gallagher and R. C. Gallo, Terminal differentiation of human promyelocytic leukemia cells induced by dimethyl sulfoxide and other polar compounds, *Proc. Natl. Acad. Sci. U. S. A.*, 1978, **75**(5), 2458–2462, DOI: 10.1073/pnas.75.5.2458.
28 I. Reigada, *et al.*, Combined Effect of Naturally-Derived Biofilm Inhibitors and Differentiated HL-60 Cells in the Prevention of Staphylococcus aureus Biofilm Formation, *Microorganisms*, 2020, **8**(11), 1757, DOI: 10.3390/microorganisms8111757.
29 M. E. Skogman, P. M. Vuorela and A. Fallarero, Combining biofilm matrix measurements with biomass and viability assays in susceptibility assessments of antimicrobials against Staphylococcus aureus biofilms, *J. Antibiot.*, 2012, **65**(9), 453–459, DOI: 10.1038/ja.2012.49.
30 M. Rubinstein and R. H. Colby, *Polymer Physics (Chemistry)*, 2003.
31 D. G. Yoon, Y. J. Kang, R. Bail and B. D. Chin, Interfaces and pattern resolution of inkjet-printed organic light-emitting diodes with a novel hole transport layer, *J. Inf. Disp.*, 2021, **22**(2), 91–98, DOI: 10.1080/15980316.2020.1866090.
32 P. He and B. Derby, Controlling Coffee Ring Formation during Drying of Inkjet Printed 2D Inks, *Adv. Mater. Interfaces*, 2017, **4**(22), 1700944, DOI: 10.1002/admi.201700944.
33 S. F. Shimobayashi, M. Tsudome and T. Kurimura, Suppression of the coffee-ring effect by sugar-assisted depinning of contact line, *Sci. Rep.*, 2018, **8**(1), 17769, DOI: 10.1038/s41598-018-35998-w.
34 D. Mampallil and H. B. Eral, A review on suppression and utilization of the coffee-ring effect, *Adv. Colloid Interface Sci.*, 2018, **252**, 38–54, DOI: 10.1016/j.cis.2017.12.008.
35 K. Knop, R. Hoogenboom, D. Fischer and U. S. Schubert, Poly(ethylene glycol) in Drug Delivery: Pros and Cons as Well as Potential Alternatives, *Angew. Chem., Int. Ed.*, 2010, **49**(36), 6288–6308, DOI: 10.1002/anie.200902672.
36 L. Tammaro, C. Saturnino, S. D'Aniello, G. Vigliotta and V. Vittoria, Polymorphic solidification of Linezolid confined in electrospun PCL fibers for controlled release in topical applications, *Int. J. Pharm.*, 2015, **490**(1–2), 32–38, DOI: 10.1016/j.ijpharm.2015.04.070.
37 M. Gaur, S. Maurya, Md. S. Akhtar and A. B. Yadav, Synthesis and Evaluation of BSA-Loaded PLGA–Chitosan Composite Nanoparticles for the Protein-Based Drug Delivery System, *ACS Omega*, 2023, **8**(21), 18751–18759, DOI: 10.1021/acsomega.3c00738.
38 N. S. Vrandečić, M. Erceg, M. Jakić and I. Klarić, Kinetic analysis of thermal degradation of poly(ethylene glycol) and poly(ethylene oxide)s of different molecular weight, *Thermochim. Acta*, 2010, **498**(1–2), 71–80, DOI: 10.1016/j.tca.2009.10.005.
39 K. Shameli, *et al.*, Synthesis and Characterization of Polyethylene Glycol Mediated Silver Nanoparticles by the Green Method, *Int. J. Mol. Sci.*, 2012, **13**(6), 6639–6650, DOI: 10.3390/ijms13066639.
40 D. Martínez-Pérez, *et al.*, 3D-printed dual drug delivery nanoparticleloaded hydrogels to combat antibiotic-resistant bacteria, *Int. J. Bioprint.*, 2023, **9**(3), 683, DOI: 10.18063/ijb.683.
41 A. J. Tande and R. Patel, Prosthetic joint infection, *Clin. Microbiol. Rev.*, 2014, **27**(2), 302–345, DOI: 10.1128/CMR.00111-13.
42 J. S. Roh and D. H. Sohn, Damage-Associated Molecular Patterns in Inflammatory Diseases, *Immune Network*, 2018, **18**(4), e27–e27, DOI: 10.4110/in.2018.18.e27.
43 E. Seebach and K. F. Kubatzky, Chronic Implant-Related Bone Infections—Can Immune Modulation be a Therapeutic Strategy?, *Front. Immunol.*, 2019, **10**, 1724, DOI: 10.3389/fimmu.2019.01724.
44 S. Franz, S. Rammelt, D. Scharnweber and J. C. Simon, Immune responses to implants - a review of the implications for the design of immunomodulatory biomaterials, *Biomaterials*, 2011, **32**(28), 6692–6709, DOI: 10.1016/j.biomaterials.2011.05.078.
45 M. Croes, *et al.*, Antibacterial and immunogenic behavior of silver coatings on additively manufactured porous titanium, *Acta Biomater.*, 2018, **81**, 315–327, DOI: 10.1016/j.actbio.2018.09.051.
46 S. Bohara and J. Suthakorn, Surface coating of orthopedic implant to enhance the osseointegration and reduction of bacterial colonization: a review, *Biomater. Res.*, 2022, **26**(1), 26, DOI: 10.1186/s40824-022-00269-3.
47 A. G. Gristina, P. T. Naylor and Q. Myrvik, in *The Race for the Surface: Microbes, Tissue Cells, and Biomaterials, presented at the Molecular Mechanisms of Microbial*, ed. Adhesion, L. Switalski, M. Höök, and E. Beachey, Springer, New York, NY, USA, 1989, pp. 177–211.
48 B. Shaqour, *et al.*, 3D-Printed Drug Delivery Systems: The Effects of Drug Incorporation Methods on Their Release and Antibacterial Efficiency, *Materials*, 2020, **13**(15), 3364, DOI: 10.3390/ma13153364.